Two-photon Excitation Fluorescent Spectral and Decay Properties of Retrograde Neuronal Tracer Fluoro-Gold

Matthew Q. Miller
Massachusetts Eye and Ear Infirmary
Iván Coto Hernández (ivan_cotohernandez@meei.harvard.edu)
Massachusetts Eye and Ear Infirmary
Jenu V. Chacko
University of Wisconsin–Madison
Steven Minderler
Massachusetts Eye and Ear Infirmary
Nate Jowett
Massachusetts Eye and Ear Infirmary

Research Article

Keywords: Fluorescence microscopy, Multiphoton fluorescence microscopy, Fluoro-Gold, Fluorescent retrograde axonal tracer, Fluorescent lifetime imaging microscopy

Posted Date: February 17th, 2021

DOI: https://doi.org/10.21203/rs.3.rs-200482/v1

Abstract

Fluoro-Gold is a fluorescent neuronal tracer suitable for targeted deep imaging of the nervous system. Widefield fluorescence microscopy enables visualization of fluoro-gold, but lacks depth discrimination. Though scanning laser confocal microscopy yields volumetric data, imaging depth is limited, and optimal single-photon excitation of fluoro-gold requires an unconventional ultraviolet excitation line. Two-photon excitation microscopy employs ultrafast pulsed infrared lasers to image fluorophores at high-resolution at unparalleled depths in opaque tissue. Deep imaging of fluoro-gold-labeled neurons carries potential to advance understanding of the central and peripheral nervous systems, yet its two-photon spectral and temporal properties remain uncharacterized. Herein, we report the relative two-photon excitation spectrum of fluoro-gold between 720 nm and 1100 nm, and its fluorescence decay rate in aqueous solution and murine brainstem tissue. We demonstrate unprecedented imaging depth of whole-mounted murine brainstem via two-photon excitation microscopy of fluoro-gold-labeled facial motor nuclei. Optimal two-photon excitation of fluoro-gold occurred at 730 nm, while maximum lifetime contrast was observed at 760 nm with mean fluorescence lifetime of 1.4 ns. Whole-mount brainstem explants were readily imaged to depths in excess of 450 μm via immersion in refractive-index matching solution.

Introduction

Retrograde neuronal labeling permits study of complex neural circuits, neuropathology, and nerve regeneration [1, 2]. In 1873, Camillo Golgi used silver staining to visualize nervous tissue under light microscopy [3]. Ramón y Cajal optimized this technique in his pioneering neuroanatomical studies underpinning the neuron doctrine [3, 4]. Weiss and Hiscoe described anterograde axonal transport in 1948 [5]. In 1971, Kristensson and Olsson demonstrated retrograde axonal transport by injecting horseradish peroxidase (HRP) into murine gastrocnemius muscle and later observing tracer in spinal cord sections [6]. Evans blue was the first fluorescent dye used for retrograde neuronal labeling; many others have since been reported [1, 7–12]. Fluorescent dyes allow high-fidelity neuronal labeling without resource-intensive immunohistochemical techniques.

Schmued and Fallon first described Fluoro-Gold™ (FG) in 1986, noting its intense fluorescence, specific labeling of damaged axons, and resistance to photobleaching [13]. Hydroxystilbamidine (OHSA) is the active fluorophore in FG, an amidine similar to DAPI, True blue, and other substances that undergo retrograde transport [14]. After axonal uptake, FG accumulates in acidic lysosomes and endosomes and is transported to the cell body where it labels cytoplasm and dendrites [13, 14]. It produces a broad fluorescence emission spectrum, with an intense yellow peak at neutral pH that is blue-shifted in acidic environments [13].

FG can be used to label neuronal cell bodies of the central and peripheral nervous systems, and shows minimal neurotoxicity at low concentrations (2–5%) [10, 13, 15–19]. Within the peripheral nervous system, FG may be employed for labeling intact motor neurons via intramuscular injection, or axotomized motor and sensory neurons via immersion of proximal nerve stumps, using conduit reservoir or crystal

application techniques [1, 9, 13, 14, 20]. Hayashi et al. demonstrated conduit reservoir delivery of FG labeled the greatest number of neurons [1]. FG is compatible with immunohistochemistry (IHC) and tissue clearing techniques [21–23].

Optimal single-photon excitation of FG is achieved using ultraviolet light. Imaging of FG-labeled specimens is typically performed using widefield fluorescence microscopy, with standard DAPI/Hoechst filter sets yielding narrow-band 365 nm excitation and long-pass filters providing broadband detection [1, 9, 13, 14, 24, 25]. However, widefield imaging lacks depth discrimination, preventing optical sectioning and high-resolution three-dimensional (3D) imaging. Confocal microscope short-wavelength excitation lasers at 405 nm are not suitable for excitation of FG [14]. Secondary tagging of FG by immunofluorescence may be employed to visualize FG using visible excitation lines of commerical confocal microscopes, though this approach is resource-intensive [26, 27].

Two-photon excitation microscopy (2PEM) is an alternative to confocal microscopy for volumetric imaging of biological tissues. Maria Goeppert-Mayer characterized the theoretical basis for 2PEM in 1931 and six decades later, Denk et al. first demonstrated the technique [28, 29]. Two-photon excitation (2PE) employs near-infrared (NIR) ultrafast laser pulses to achieve simultaneous absorption of two low-energy photons by a fluorophore typically excited by a single higher-energy photon. Multiphoton NIR excitation is possible for manifold fluorophores, including many which are not suitably excited using visible light [30, 31]. Use of NIR excitation in the optical window of biological tissue in 2PEM permits microscale resolution of labeled-structures in highly-scattering thick tissues [32]. Owing to the quadratic dependence of fluorescence signal on excitation intensity in 2PEM, out-of-plane fluorescence is largely avoided, providing enhanced axial resolution compared to scanning laser confocal microscopy [28]. Under ideal conditions, confocal microscopy can image tissues at depths up to 100 μm, while depths up to 1 mm have been reported with 2PEM [33–36]. Though the 2PE spectral properties of many fluorescent dyes have been documented, the 2PEM excitation spectra of FG has not been heretofore characterized [37].

Due to FG's broad fluorescent emission spectrum, spectral overlap with other fluorophores is common and can hinder multicolor imaging. Several approaches may be employed for multicolor imaging of FG-labeled specimens. In single-photon imaging, UV excitation of FG may enable its separation from fluorophores not excited by UV light [15, 38]. Fluorescence lifetime imaging (FLIM) obtains images based on fluorophore decay rate in lieu of fluorescent intensity, yielding means to resolve fluorescent labels with overlapping absorption and emission spectra [39–41]. FLIM necessitates use of short-pulse excitation lasers, and may be implemented using single or multiphoton excitation techniques. Ultrafast pulsed lasers used for 2PEM are well-suited for FLIM; such microscope systems can readily be upgraded to enable FLIM [39]. A priori knowledge of specific decay rates of various fluorophores enables selection of optimal candidates for multi-label experiments. Heretofore, the decay rate of FG has not been characterized.

Herein, we characterize the 2PE spectra and fluorescent lifetime distribution of FG in aqueous solution and murine facial motor nuclei. We then demonstrate the utility of 2PEM for high-throughput deep

volumetric imaging of FG-labeled mammalian neurons.

Results

The 2PE fluorescent spectral and decay properties for FG in aqueous solution (2% w/v in distilled water) and murine brainstem tissue were determined using a commercial multiphoton microscope, powered by a tunable mode-locked Ti:Sapphire laser between 720–1100 nm (Fig. 1A-C). A second commerical multiphoton microscope, powered by a tunable dual-output Ytterbium laser between 720–1300 nm, was employed to verify the quadratic dependence of FG's fluorescence emission and absense of fluorescent signal between 1100 nm and 1300 nm (Supplementary Fig. S1). Maximal excitation for FG in brainstem tissue (adjusted for background tissue fluorescence) occurred at 730 nm (Fig. 1D).

The apparent fluorescence lifetime of FG-labeled facial motoneurons was measured at 1.4 ns using fitting procedures (Fig. 1E). Optimal excitation to maximize lifetime contrast between FG-labeled cell bodies and background brainstem tissue fluorescence was 760 nm (Fig. 1F). The fluorescence lifetime of FG in aqueous solution and brainstem tissue followed a bi-exponential distribution (Fig. 1G, 1H). Two components were resolved, a high-intensity fluorescent decay (a_1) with a lifetime of less than 100 ps, and a low-intensity decay (a_2) with a lifetime of 2.3 ns (Figs. 1E, 1G). The high-intensity and shorter lifetime component had a decay of 21.2 ps with a green-yellow filter (550/88 nm), and 39.2 ps without a filter. The background lifetime was measured at 1.35 ns (averaged across all excitation wavelengths, Supplementary Fig. S2). Fractional 2PE spectra of high and low-intensity decay components of FG in aqueous solution were closely related, both having a maximum at 730 nm (Fig. 1H).

Immersion of transected murine extratemporal facial nerve main trunk in FG for 10 minutes resulted in excellent visualization of intermediate, lateral, and dorsolateral facial subnuclei within 6 days (Fig. 2). For multi-label experiments, immersion of transected murine facial nerve buccal and zygomatic branches in FG and Fluoro-Ruby (FR), respectively, yielded facial motor subnuclei-specific labeling (Supplementary Fig. S3).

2PEM imaging of murine brainstem tissue sections demonstrated superior lateral and axial resolution at 25x and 100x magnification compared to widefield fluorescence microscopy (Fig. 3). Dendrites and subcellular structures were visualized using 2PEM, whereas these structures were poorly resolved on widefield microscopy (Fig. 3). Excellent optical sectioning and 3D reconstruction of the facial nucleus were performed on sectioned and whole-mount tissues (Figs. 3 and 4). High-resolution imaging depths in excess of 450 μm were achieved in whole-mount tissue, using refractive index matching and increasing optical power with depth to compensate for signal attenuation. Machine-learning based image segmentation was used for automated quantification of labeled cell bodies (Fig. 4).

Discussion

The present study is the first to characterize the 2PE fluorescent spectral and lifetime characteristics of FG, a fluorescent dye considered by many as the “gold-standard” for retrograde neuronal labeling [27]. FG’s maximum 2PE occurs at 730 nm, approximately twice its peak single-photon excitation [1, 13]. We demonstrated improved image resolution and optical sectioning by means of 2PEM over conventional approaches, with near perfect power-squared dependence (Supplementary Fig. S1) [31, 39]. The achieved resolution by 2PEM was sufficient for visualization of dendrites and subcellular structures (Fig. 3). The utility of 2PEM in resolving FG-labeled dendrites sufficient for quantification carries relevance to the field of neuropathology, as dendritic number and morphology changes are associated with neurodegenerative diseases [42]. The FG-labeled subcellular structures resolved by 2PEM likely represent dye accumulation in neuronal endosomes and lysosomes (Fig. 3H) [14].

Imaging depth of 2PEM is limited by optical aberration and light attenuation caused by absorption and scattering of light within thick biological samples [28]. Spherical aberration, which is caused by optical inhomogeneities within the sample and the immersion medium, blurs images and causes loss of detail in deep tissue [43]. Several tissue clearing techniques have been proposed to increase imaging depth of fixed tissues; an excellent review of these techniques was published by Richardson and Lichtman [44–46]. The present work used optical clearing via simple immersion in EasyIndex (commercially-available PROTOS) refractive index matching solution due to its ease of use, effectiveness, and low-cost compared to other tissue clearing techniques [45, 47, 48]. Herein, whole-mount murine brainstem was imaged at depths greater than 450 μm using a glycerol-immersion objective lens within a refractive index matching solution (Fig. 3). In contrast, imaging depths of FG-labeled murine facial motor nuclei were limited to 150 μm using a water immersion objective lens without refractive index matching.

Imaging of fluorescent labels in nervous tisues may be complicated by lipofuscin-associated autofluorescence. Lipofuscin demonstrates broad excitation and emission spectra, often resulting in poor signal-to-background ratio impacting fluorescence imaging quality. Though pre-treatment of nervous system specimens with sudan black or cupric sulfate may reduce background lipofuscin fluorescence, adequate quenching while maintaining suitable fluorophore fluorescence is challenging [49, 50]. Herein, we observed an average fluorescence lifetime of 1.4 ns for FG, comprised of a high-intensity fluorescent decay component with a lifetime of less than 100 ps, and a low-intensity component having a lifetime of 2.3 ns. The fluorescence lifetime of lipofuscin has been measured between 500–650 ps in tissue [49, 51–53]. The large difference between fluorescence lifetimes of FG and lipofuscin indicates they are readily separable using FLIM, demonstrated herein by the improvement in signal-to-background ratio with FLIM of FG-labeled murine brainstem (Fig. 1A, 1B).

This report has several limitations. The present work did not measure the absolute two-photon absorption spectrum of FG, necessary for direct comparison of its brightness against other fluorescent dyes [31, 54]. TPE spectra and lifetimes for other common retrograde neuronal tracers including FR should be established to facilitate multi-label studies. Multi-label retrograde neuronal tracer experiments using

2PEM with FLIM for deep multicolor volumetric imaging could facilitate study of the somatotopic organization of neuronal circuits [55, 56]. Protocols for 2PEM of FG in tissues cleared by solvents could be developed. FG is compatible with lipid-clearing techniques, which can extend imaging depth to span the entire thickness of the mouse cortex [23]. The present study utilized image analysis software for segmentation and automated counts of facial neuron cell bodies (Fig. 4). Prior studies have sectioned brainstem tissue and manually counted labeled cell bodies in the murine facial nucleus; a time- and resource-intensive method [9, 57]. Future studies should evaluate the accuracy of automated cell body counts in volumetric imaging against tissue sectioning and manual cell counts.

Materials And Methods

Materials

FG (Fluorochrome, Denver, CO) was used for widefield, 2PEM, and FLIM. A concentration of 2% FG (w/v in distilled water) was used to minimize neurotoxicity, and employed for animal experiments and characterization of dye properties in acqueous solution. FR (10% w/v in distilled water, Invitrogen, Carlsbad, CA) was used for facial subnuclei labeling to demonstrate the utility of multi-labeling techniques incorporating FG. Tissue sections were mounted in Fluoromount-G (SouthernBiotech, Birmingham, AL). EasyIndex (Life Canvas Technologies, Cambridge, MA) was used for refractive index matching.

Animal Surgeries

Two female C57 adult mice (7 weeks) and one 4-week old female Lewis rat were used in the present study. All animal surgeries were performed in accordance with the National Institutes of Health Guide for the Care and Use of Laboratory Animals, and with approval by the Massachusetts Eye and Ear Animal Care Committee (ACC Protocol # 16 – 006, IRBNet ID 884247). This study was carried out in compliance with the ARRIVE guidelines. Five uL of 2% FG was delivered to the transected main facial nerve trunk of the C57 mice via the conduit reservoir technique (Fig. 2). In the Lewis rat, 5 µL FG was delivered to the transected facial nerve buccal branch, and 5 uL 10% FR was delivered to the transected zygomatic branch to demonstrate labeling of facial subnuclei.

Procedures were performed under isoflurane anesthesia, 1–3% maintenance dosing in 1 L/min O_2. Buprenorphine (0.05 mg/kg subcutaneously) and meloxicam (1.0 mg/kg subcutaneously) were administered prior to skin incision. A 1 cm infra-auricular incision was made on the left, and skin-muscle flaps were elevated. The exorbital lacrimal gland was retracted to expose the proximal pes anserinus and main trunk. The main trunk was meticulously dissected circumferentially using the operating microscope at 25x magnification. Care was taken to prevent crush injury. The nerve was transected and the proximal stump was immersed in a pipette tip containing 5 µL of dye solution for 10 minutes. The wound bed was irrigated with saline and closed in a single layer using 4 – 0 absorbable suture (Polysyn, Sharpoint, Westwood, MA). Animals were recovered from general anesthesia and returned to their cages. A single postoperative dose of meloxicam was given 24 hours post-procedure. The identical procedure was

performed for the Lewis rat, except the buccal and zygomatic facial nerve branches were transected for delivery of FG and FR, respectively.

Tissue Harvest

After a six-day survival period, animals underwent CO_2 euthanasia and cardiac perfusion using 2% phosphate-buffered paraformaldehyde fixative (PFA) solution. Animal heads were placed in 2% PFA overnight, then underwent brainstem harvest at the level of the facial nucleus. The intracranial facial nerve was used as a landmark for facial motor nucleus identification. Specimens were cryo-protected in 30% sucrose for 24 hours prior to embedding in optimal cutting temperature (OCT) compound and coronal cyrosectioning at 40 µm (Leica CM3050 S, Leica Biosystems, Buffalo Grove, IL). Slides were mounted using Fluoromount-G to minimize photobleaching during subsequent imaging. Whole-mount brainstems were imaged following overnight fixation in 2% PFA and six-hour incubation in 100% EasyIndex on a shaker at room temperature.

Tissue Imaging

Comparison of widefield and 2PEM imaging was performed on a commercial multiphoton microscope (TrimScope II, LaVision Biotech) powered by a dual-output femtosecond laser (Insight X3, SpectraPhysics) at 760 nm. Images were acquired with a set of galvanometer mirrors and piezo XYZ-stage for large-field volumetric imaging. For thick sections, a water-immersion objective lens with correction collar (N25X-APO-MP1300, Nikon) was employed. For whole-mount imaging, optical clearing was achieved using a glycerol-immersion objective lens (CLr Plan-Neofluar 20x, Carl Zeiss) and refractive index matching solution (EasyIndex). A dichroic mirror at 700 nm was employed to separate excitation and emission light, and a second dichroic mirrior at 435 nm used to split the emission light in the non-descanned detection path. Fluorescent signal was filtered (Semrock 525/50 nm) and collected using a GaAsP photomultiplier tube (H 7422-40, Hamamatsu). Image acquisition was averaged four times to improve signal-to-noise ratio. The quadratic dependence of 2PE fluorescence was assessed from fluorescent images, by measurement of the variation of fluorescence intensity with increasing excitation intensity. Widefield epifluorescent imaging was performed using the multiphoton microscope stage, broadband light-emitting diode excitation (pE-300 ultra, CoolLED, Andover, England), and a monochrome Zyla 4.2 sCMOS camera (Andor Technology Ltd, Belfast, Northern Ireland). Microscope control was achieved via open-source software (LaVision BioTec ImSpector Software).

FLIM data was acquired using an upright multiphoton microscope (Ultima, Bruker Microscopy, Middleton, WI) coupled to an ultrafast tunebale NIR laser (Insight DS, Spectra Physics, CA) between 720 nm and 1100 nm. Images were collected using a 10X/0.5NA objective lens (CFI Super Fluor, Nikon). Optical power was continuously measured during experiments using a silicon-based photodetector power meter (918D-SL-OD3R, Newport, MKS, CA), digitized using an open-source microcontroller (Arduino UNO, Arduino, Ivrea, Italy), and the digital laser power value was added to the metadata of the file using PrairieView software (Bruker, Billerica, MA). Fluorescence intensity and lifetime distribution analyses were performed on dye solution (2% W/V in distilled water) and FG-labeled brainstem sections.

Dye solutions were loaded into sealed glass capillary tubes and imaged over 10 nm wavelength intervals between 720 nm and 1100 nm. Fast-electronics comprising a hybrid detector (HPM-100-40, Becker&Hickl, Berlin, Germany) and time-correlation single-photon counting card (SPC-150, Becker&Hickl, Berlin, Germany) encoded photon arrivals times. Timing data of individual photons were binned and mathematically fit to double-exponential curves using commercial software (SPCImage, Becker&Hickl, Berlin, Germany). Resultant lifetime and intensity analyses and spectral plots for specific wavelengths were performed using ImageJ [58].

Image Processing

Facial motor neuron cell body counts were quantified from original 3D data sets using commercial machine learning software (Aivia v9.5, SVision Technologies, Bellevue, WA). A random forest pixel classifier was trained by painting examples of cell body signal and background signal [59]. This classifier was used to generate a signal channel in Aivia's 3D object mesh recipe consol to highlight and segment neuronal cell bodies. The object meshes were generated in a region of interest and adjusted in a iterative manner, during which morphological smoothing was performed, minimum object edge intensity defined, and holes filled until a satisfactory result was obtained. The segmentation parameters were then applied to the entire volume to generate a channel highlighting pixels comprising cell bodies.

Declarations

Acknowledgments

The authors thank Doug Matthews from SVision Technologies LLC for technical assistance with Aivia software.

Funding Support: This work was supported by the National Institutes of Health (NIH) NIDCR 1F32DE029964-01; NINDS 2 R01 NS071067- 06A1; Charles H. Hood Foundation Child Health Research Award; Berthiaume Family

Author contributions

M.Q.M performed the experiments, conceived the study, and wrote the manuscript. I.C.H. performed the experiments, conceived the study, and critically reviewed the manuscript. J.V.C. performed the FLIM experiments and critically reviewed the manuscript. S.M. performed the experiments. N.J. conceived the study and critically reviewed the manuscript.

Additional information

Competing interests: The authors declare no competing interests.

References

1. Hayashi, A., et al., *Retrograde labeling in peripheral nerve research: it is not all black and white.* J Reconstr Microsurg, 2007. **23**(7): p. 381-9.
2. Schmued, L.C., *Development and application of novel histochemical tracers for localizing brain connectivity and pathology.* Brain Res, 2016. **1645**: p. 31-5.
3. Grant, G., *How the 1906 Nobel Prize in Physiology or Medicine was shared between Golgi and Cajal.* Brain Res Rev, 2007. **55**(2): p. 490-8.
4. Glickstein, M., *Golgi and Cajal: The neuron doctrine and the 100th anniversary of the 1906 Nobel Prize.* Curr Biol, 2006. **16**(5): p. R147-51.
5. Weiss, P. and H.B. Hiscoe, *Experiments on the mechanism of nerve growth.* J Exp Zool, 1948. **107**(3): p. 315-95.
6. Kristensson, K. and Y. Olsson, *Retrograde axonal transport of protein.* Brain Res, 1971. **29**(2): p. 363-5.
7. Kristensson, K., *Transport of fluorescent protein tracer in peripheral nerves.* Acta Neuropathol, 1970. **16**(4): p. 293-300.
8. van der Kooy, D. and H.G. Kuypers, *Fluorescent retrograde double labeling: axonal branching in the ascending raphe and nigral projections.* Science, 1979. **204**(4395): p. 873-5.
9. Choi, D., D. Li, and G. Raisman, *Fluorescent retrograde neuronal tracers that label the rat facial nucleus: a comparison of Fast Blue, Fluoro-ruby, Fluoro-emerald, Fluoro-Gold and DiI.* J Neurosci Methods, 2002. **117**(2): p. 167-72.
10. Novikova, L., L. Novikov, and J.O. Kellerth, *Persistent neuronal labeling by retrograde fluorescent tracers: a comparison between Fast Blue, Fluoro-Gold and various dextran conjugates.* J Neurosci Methods, 1997. **74**(1): p. 9-15.
11. Puigdellívol-Sánchez, A., et al., *On the use of fast blue, fluoro-gold and diamidino yellow for retrograde tracing after peripheral nerve injury: uptake, fading, dye interactions, and toxicity.* J Neurosci Methods, 2002. **115**(2): p. 115-27.
12. Richmond, F.J., et al., *Efficacy of seven retrograde tracers, compared in multiple-labelling studies of feline motoneurones.* J Neurosci Methods, 1994. **53**(1): p. 35-46.
13. Schmued, L.C. and J.H. Fallon, *Fluoro-Gold: a new fluorescent retrograde axonal tracer with numerous unique properties.* Brain Res, 1986. **377**(1): p. 147-54.
14. Wessendorf, M.W., *Fluoro-Gold: composition, and mechanism of uptake.* Brain Res, 1991. **553**(1): p. 135-48.
15. Harsh, C., S.J. Archibald, and R.D. Madison, *Double-labeling of saphenous nerve neuron pools: a model for determining the accuracy of axon regeneration at the single neuron level.* J Neurosci Methods, 1991. **39**(2): p. 123-30.
16. Madison, R.D., S.J. Archibald, and T.M. Brushart, *Reinnervation accuracy of the rat femoral nerve by motor and sensory neurons.* J Neurosci, 1996. **16**(18): p. 5698-703.

17. Tiwari, E., et al., *Nerve transfer for restoration of lower motor neuron-lesioned bladder and urethra function: establishment of a canine model and interim pilot study results.* J Neurosurg Spine, 2019. **32**(2): p. 258-268.
18. Akintunde, A. and D.F. Buxton, *Differential sites of origin and collateralization of corticospinal neurons in the rat: a multiple fluorescent retrograde tracer study.* Brain Res, 1992. **575**(1): p. 86-92.
19. Sharma, S., et al., *Parallel descending dopaminergic connectivity of A13 cells to the brainstem locomotor centers.* Sci Rep, 2018. **8**(1): p. 7972.
20. Pieribone, V.A. and G. Aston-Jones, *The iontophoretic application of Fluoro-Gold for the study of afferents to deep brain nuclei.* Brain Res, 1988. **475**(2): p. 259-71.
21. Ju, G., Z.S. Han, and L.Z. Fan, *Fluorogold as a retrograde tracer used in combination with immunohistochemistry.* J Neurosci Methods, 1989. **29**(1): p. 69-72.
22. Geddes, S.D., et al., *Target-specific modulation of the descending prefrontal cortex inputs to the dorsal raphe nucleus by cannabinoids.* Proc Natl Acad Sci U S A, 2016. **113**(19): p. 5429-34.
23. Wang, P., et al., *Feasibility of commonly used fluorescent dyes and viral tracers in aqueous and solvent-based tissue clearing.* Neurosci Lett, 2020. **737**: p. 135301.
24. van Oterendorp, C., et al., *Quantification of retrograde axonal transport in the rat optic nerve by fluorogold spectrometry.* PLoS One, 2012. **7**(6): p. e38820.
25. Chen, L., et al., *Motor fiber organization in the extratemporal trunk of the facial nerve in rats: A retrograde Fluoro-Gold study.* Exp Ther Med, 2012. **4**(5): p. 844-848.
26. Freedman, L.J. and H. Yi, *Confocal imaging of the retrograde tracer fluoro-gold using a non-ultraviolet laser.* Brain Res Bull, 1993. **31**(6): p. 749-51.
27. Lanciego, J.L. and F.G. Wouterlood, *Neuroanatomical tract-tracing techniques that did go viral.* Brain Struct Funct, 2020. **225**(4): p. 1193-1224.
28. Denk, W., J.H. Strickler, and W.W. Webb, *Two-photon laser scanning fluorescence microscopy.* Science, 1990. **248**(4951): p. 73-6.
29. Göppert-Mayer, M., *Über Elementarakte mit zwei Quantensprüngen.* Annalen der Physik, 1931. **401**(3): p. 273-294.
30. Albota, M.A., C. Xu, and W.W. Webb, *Two-Photon Fluorescence Excitation Cross Sections of Biomolecular Probes from 690 to 960 nm.* Appl Opt, 1998. **37**(31): p. 7352-6.
31. Webb, C.X.a.W.W., *Measurement of two-photon excitation cross sections of molecular fluorophores with data from 690 to 1050 nm.* J. Opt. Soc. Am. , 1996. **13**: p. 481-491.
32. Smith, A.M., M.C. Mancini, and S. Nie, *Second window for in vivo imaging.* Nature nanotechnology, 2009. **4**(11): p. 710-711.
33. Theer, P., M.T. Hasan, and W. Denk, *Two-photon imaging to a depth of 1000 microm in living brains by use of a Ti:Al2O3 regenerative amplifier.* Opt Lett, 2003. **28**(12): p. 1022-4.
34. Helmchen, F. and W. Denk, *Deep tissue two-photon microscopy.* Nat Methods, 2005. **2**(12): p. 932-40.

35. Svoboda, K., et al., *In vivo dendritic calcium dynamics in neocortical pyramidal neurons.* Nature, 1997. **385**(6612): p. 161-5.
36. Helmchen, F., et al., *In vivo dendritic calcium dynamics in deep-layer cortical pyramidal neurons.* Nat Neurosci, 1999. **2**(11): p. 989-96.
37. Ricard, C., et al., *Two-photon probes for in vivo multicolor microscopy of the structure and signals of brain cells.* Brain Struct Funct, 2018. **223**(7): p. 3011-3043.
38. Zele, T., J. Sketelj, and F.F. Bajrović, *Efficacy of fluorescent tracers in retrograde labeling of cutaneous afferent neurons in the rat.* J Neurosci Methods, 2010. **191**(2): p. 208-14.
39. Benninger, R.K. and D.W. Piston, *Two-photon excitation microscopy for the study of living cells and tissues.* Curr Protoc Cell Biol, 2013. **Chapter 4**: p. Unit 4.11.1-24.
40. Levitt, J.A., et al., *Fluorescence lifetime and polarization-resolved imaging in cell biology.* Curr Opin Biotechnol, 2009. **20**(1): p. 28-36.
41. Stringari, C., et al., *Phasor approach to fluorescence lifetime microscopy distinguishes different metabolic states of germ cells in a live tissue.* Proc Natl Acad Sci U S A, 2011. **108**(33): p. 13582-7.
42. Mancuso, J.J., et al., *Methods of dendritic spine detection: from Golgi to high-resolution optical imaging.* Neuroscience, 2013. **251**: p. 129-40.
43. Schwertner, M., et al., *Measurement of specimen-induced aberrations of biological samples using phase stepping interferometry.* J Microsc, 2004. **213**(1): p. 11-9.
44. Hama, H., et al., *Scale: a chemical approach for fluorescence imaging and reconstruction of transparent mouse brain.* Nat Neurosci, 2011. **14**(11): p. 1481-8.
45. Chung, K., et al., *Structural and molecular interrogation of intact biological systems.* Nature, 2013. **497**(7449): p. 332-7.
46. Richardson, D.S. and J.W. Lichtman, *Clarifying Tissue Clearing.* Cell, 2015. **162**(2): p. 246-257.
47. Lee, E., et al., *ACT-PRESTO: Rapid and consistent tissue clearing and labeling method for 3-dimensional (3D) imaging.* Scientific Reports, 2016. **6**(1): p. 18631.
48. Yang, B., et al., *Single-cell phenotyping within transparent intact tissue through whole-body clearing.* Cell, 2014. **158**(4): p. 945-958.
49. Schnell, S.A., W.A. Staines, and M.W. Wessendorf, *Reduction of lipofuscin-like autofluorescence in fluorescently labeled tissue.* J Histochem Cytochem, 1999. **47**(6): p. 719-30.
50. Oliveira, V.C., et al., *Sudan Black B treatment reduces autofluorescence and improves resolution of in situ hybridization specific fluorescent signals of brain sections.* Histol Histopathol, 2010. **25**(8): p. 1017-24.
51. Doyle, K.P., et al., *Working with GFP in the brain.* Biotechniques, 2003. **34**(3): p. 492-4.
52. Corrêa, F.M., et al., *Fluorescent probes of alpha- and beta-adrenergic and opiate receptors: biochemical and histochemical evaluation.* Neurosci Lett, 1980. **16**(1): p. 47-53.
53. Sun, Y., et al., *Autofluorescence Lifetime Imaging of Lipofuscin and Melanin in Retinal Pigment Epithelium Cells.* Investigative Ophthalmology & Visual Science, 2007. **48**(13): p. 2965-2965.

54. Xu, C. and W.R. Zipfel, *Multiphoton excitation of fluorescent probes.* Cold Spring Harb Protoc, 2015. **2015**(3): p. 250-8.
55. Stringari, C., et al., *Multicolor two-photon imaging of endogenous fluorophores in living tissues by wavelength mixing.* Sci Rep, 2017. **7**(1): p. 3792.
56. Laviv, T., et al., *Simultaneous dual-color fluorescence lifetime imaging with novel red-shifted fluorescent proteins.* Nat Methods, 2016. **13**(12): p. 989-992.
57. Ashwell, K.W., *The adult mouse facial nerve nucleus: morphology and musculotopic organization.* J Anat, 1982. **135**(Pt 3): p. 531-8.
58. Schneider, C.A., W.S. Rasband, and K.W. Eliceiri, *NIH Image to ImageJ: 25 years of image analysis.* Nat Methods, 2012. **9**(7): p. 671-5.
59. Coto Hernández, I., et al., *Label-free histomorphometry of peripheral nerve by stimulated Raman spectroscopy.* Muscle Nerve, 2020. **62**(1): p. 137-142.

Figures

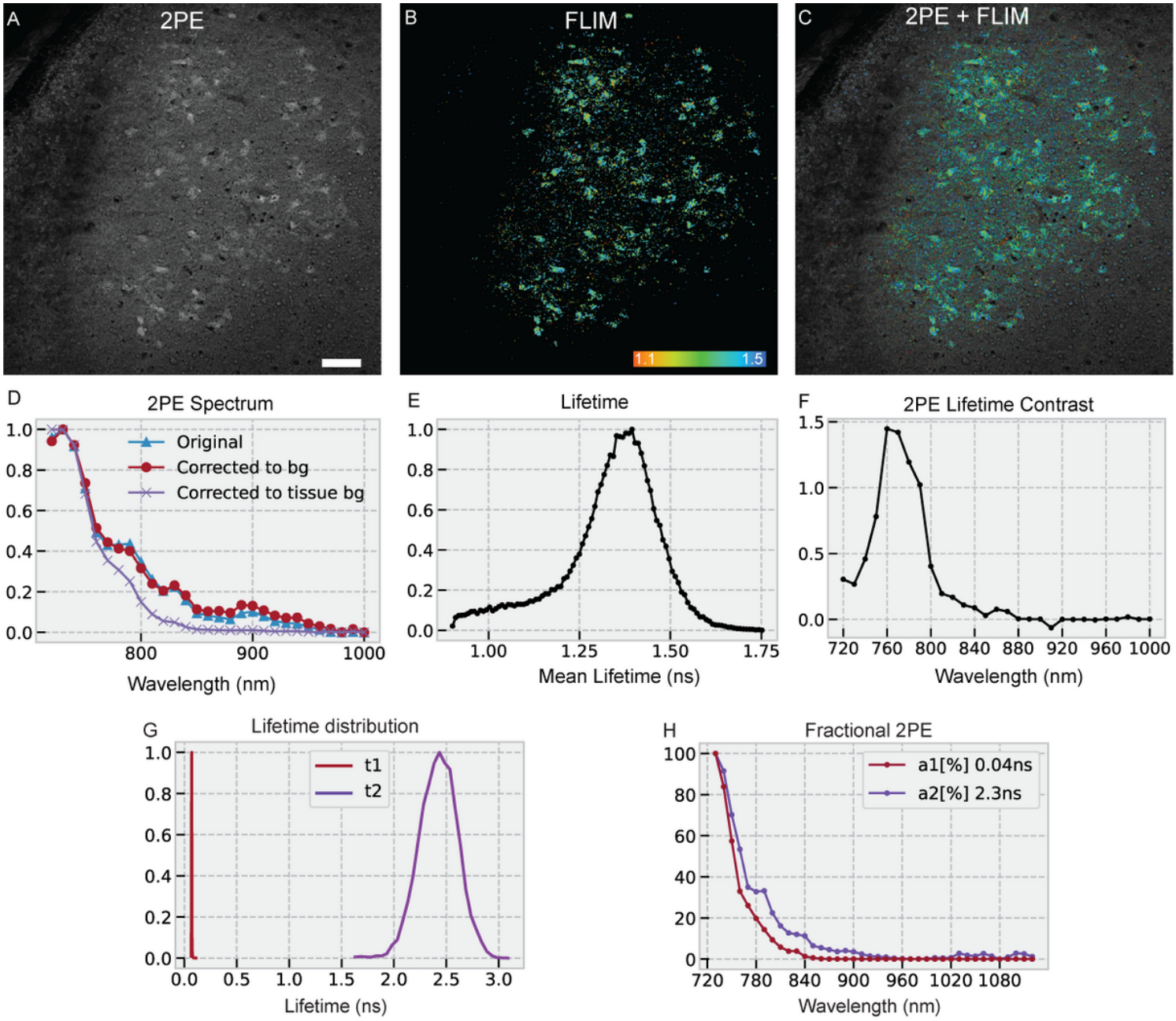

Figure 1

Two-photon excitation (2PE) fluorescence spectral and lifetime properties of Fluoro-Gold (FG) in tissue and aqueous solution. (A) 2PE fluorescence imaging of murine facial motor nucleus labeled with FG at 730 nm. (B) FLIM image. (C) FLIM image on top of raw data. (D) 2PE spectra in brainstem tissue have a maximum at 730 nm. (E) The apparent lifetime distribution of FG was 1.4 ns in paraformaldehyde-fixed murine brainstem. (F) Maximum contrast between FG and background tissue 2PE lifetime fluorescence occurred at 760 nm. (G) 2PE decay of FG in aqueous solution fit to a bi-exponential decay model demonstrates two different lifetime components; t1 < 100 ps and t2 = 2.3ns. (H) The relative 2PE spectra of FG in aqueous solution of the two components, a1 and a2. These values give the fractional excitation of the species, normalized to total photons emitted. Scale bar 100 um.

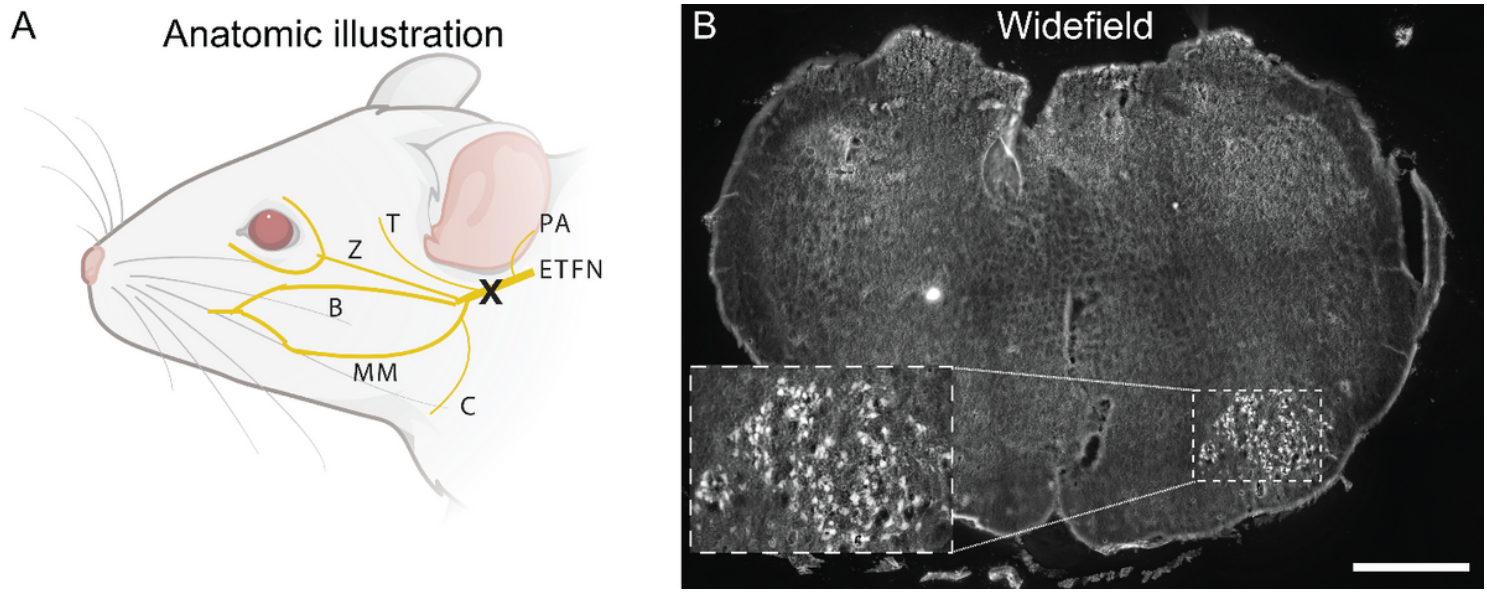

Figure 2

Retrograde labeling of murine facial motor nucleus with Fluoro-Gold. (A) The extratemporal main trunk of the facial nerve was transected distal to the auricular branches, and immersed in Fluoro-Gold for 10 minutes (transection site marked by X). (B) Visualization of left facial motor nucleus by widefield fluorescence microscopy; robust staining of all subnuclei exluding the medial subnucleus of the auricular branches is noted. Scale bar 1 mm. ETFN=extratemporal facial nerve. PA=postauricular branch. MM=marginal mandibular branch. C=cervical branch. B=buccal branch. Z=zygomatic branch. T=temporal branch. Diagram created using Biorender.

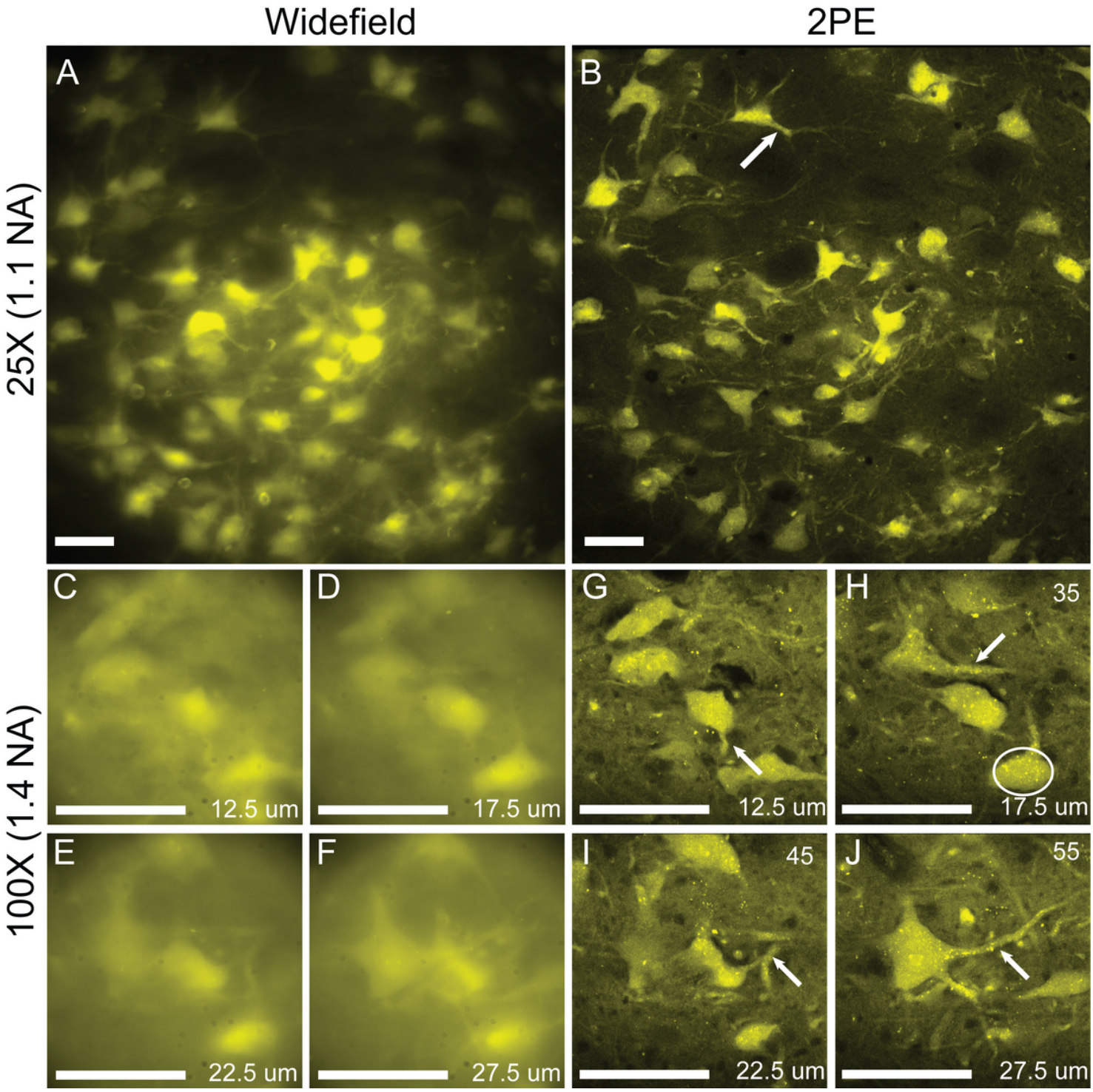

Figure 3

Widefield versus two-photon excitation microscopy of Fluoro-Gold-labeled 40 µm thick murine facial motor nuclei sections. Superior image resolution and optical sectioning is noted for 2PEM at 25x (A-B) and 100x (C-J) magnification. Excellent visualization of FG accumulation in dendrites (white arrows) and punctate subcellular accumulations (white circle in panel H) is observed within 2PEM images. Scale bar 50 µm.

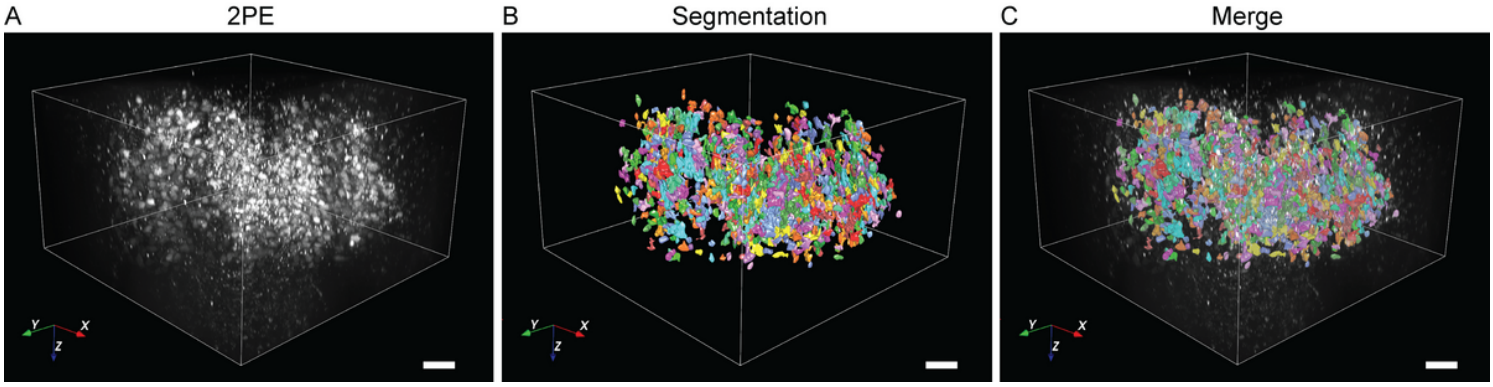

Figure 4

Deep two-photon excitation microscopy imaging of whole-mount FG-labeled murine facial motor nucleus. (A) Three-dimensional reconstruction of x-y-z tile scans. (B) Neuron cell body segmentation; automated count demonstrated 875 labeled cell bodies. (C) Merged segmented and raw data. Scale bar 100 um. Reconstructions and segmentation performed using commercial software (Aivia v9.5, SVision, Bellevue, WA).

Supplementary Files

This is a list of supplementary files associated with this preprint. Click to download.

- FinalSupplementaryMateralFGManuscript.docx